ACS OMEGA

http://pubs.acs.org/journal/acsodf

Article

Effect of Reaction Parameters on Catalytic Pyrolysis of Waste Cooking Oil for Production of Sustainable Biodiesel and Biojet by Functionalized Montmorillonite/Chitosan Nanocomposites

Hanan A. Ahmed, Amal A. Altalhi, Sameh A. Elbanna, Hend A. El-Saied, Ahmed A. Farag, Nabel A. Negm,* and Eslam A. Mohamed*

Cite This: *ACS Omega* 2022, 7, 4585−4594

Read Online

ACCESS | Metrics & More | Article Recommendations

ABSTRACT: The use of waste oils as pyrolysis feedstocks to manufacture high-grade biofuels has prompted researchers to focus on developing renewable energy to overcome the depletion of fossil fuel supplies and the global warming phenomena. Because of their high hydrogen and volatile matter concentration, waste oils are ideal raw materials for the production of biofuels. It is challenging to attain satisfactory results with conventional methods, such as transesterification, gasification, solvent extraction, and hydrotreating due to flaws such as high energy demand, long time, and high operating costs. Catalytic pyrolysis of waste edible oils was employed as a resource for the generation of biodiesel. The application of the catalytic cracking process has the potential to alleviate the existing situation. In this study of catalytic cracking conversion of waste cooking oil to produce different biofuels, grades were investigated using two heterogeneous catalysts. The catalysts were activated montmorillonite (PAMMT) clay and its modified form using a chitosan biopolymer (PAMMT-CH) nanocomposite. The catalysts were identified using infrared spectroscopy, X-ray diffraction patterns, transmittance electron microscopy images, surface area, and thermal stability. The catalysts were tested for their performances using different amounts (0.1−1% by weight) at a temperature assortment of 200−400 °C during a time range of 60−300 min. The experimental studies were carried out in a batch reactor. GC mass spectra were used to investigate the catalytic cracking products. Fractional distillation is used to separate the final products from various reaction conditions. The physicochemical properties of resulting biofuels were profiled by quantifying their densities, viscosities, specific gravities, pour points, flash and fire points, cetane numbers, carbon and ash residues, and sulfur contents. The optimum conditions of the yield product were 300 and 400 °C, catalyst weights of 0.7 and 0.8% w/v, and reaction times of 120 and 180 min concerning the (PAMMT) and (PAMMT-CH) nanocomposite, respectively. The determined properties were located within the limits of the specific standards of ASTM specifications. As a result, the PAMMT nanocomposite produced biofuel comparable to biodiesel according to ASTM specifications, while the PAMMT-CH nanocomposite produced biofuel comparable to biojet.

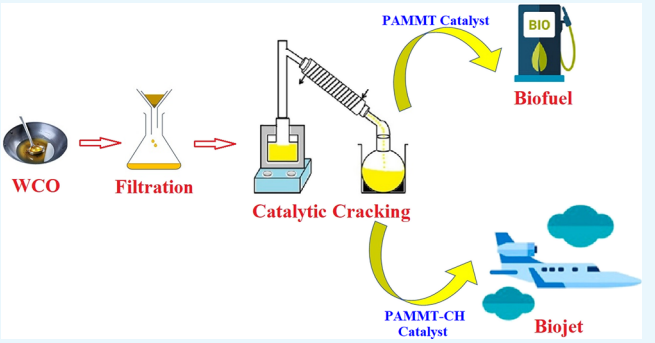

INTRODUCTION

Recently, the global focus has shifted to energy security, where biomass can play an important role in the energy matrix, which includes economic, political, food security, technological, and environmental considerations.[1] Shortly, the conversion of biomass such as waste cooking oil (WCO) to biofuel,[2] which combines biochemical and thermochemical technologies,[3] is regarded as one of the primary green substitutes for the production of biochemical and biofuels.[4] Between these biofuels, one that has received a lot of attention is the replacement for traditional jet fuel, recognized as renewable biojet fuel.[5] Biojet fuel typically has a positive influence on sustainability, whereas[6] traditional flying fuel affects the atmosphere through a multiplicity of emissions such as NO_x, SO_x, and CO_2; this leads to a change in climate and ozone layer reduction.[7] Biojet fuel can replace conventional jet fuel without requiring changes to the design of existing aircraft engines or fuel distribution systems.[8] Biojet fuel has numerous characteristics that distinguish it from conventional jet fuel. Paths have been accepted by the American Society for Testing

Received: November 22, 2021
Accepted: January 14, 2022
Published: January 31, 2022

and Materials (ASTM).[9] Biojet is produced without using aromatic compounds in contrast with conventional jet fuel. Although aromatic compounds are responsible for CO_2 emissions during combustion, they must be present within a certain range in traditional jet fuel to prevent engine leakage and to confirm certain legislative properties such as viscosity and density.[10] Because of its restrictions on food use, low cost, and suitability for fuel production, WCO is one of the most prudent sources of energy.[11] These materials are usually discarded from cafeterias, but they have the potential to play a significant role in biofuel production. The use of WCO in biofuel production addresses environmental issues regarding the handling of waste. Furthermore, the type of biofuel production process used with this feedstock can have a significant impact on biofuel's overall financial viability.[12] There are generally two ways to produce diesel from waste cooking oil: esterification, which converts triglycerides to methyl-esters with the help of methanol, and thermal treatment, which includes thermal cracking, catalysts, and hydrotreating. Currently, thermochemical conversions such as pyrolysis, which can be accomplished by either thermal pyrolysis or catalytic cracking, are being used. Due to the necessity of high efficacy for biofuel production as well as separation from the raw resources, selecting a catalyst for such a process is very important. Most homogeneous catalysts are active in biofuel processes, but they are sensitive to water and FFAs in the feedstock, which might result in undesirable soap as a byproduct.[13] This byproduct complicates final product separation and lowers the activity of the catalyst, and a vast environmentally unfavorable water washing procedure is necessary.[14] Heterogeneous catalysts can overcome these issues when compared to homogeneous catalysts. So far, several heterogamous catalysts for biofuel generation have been studied, including zeolite,[15] alkaline earth oxides,[16] ion-exchange resins,[17] inorganic-oxide solid acids, supported alkaline or alkaline earth metals, and supported noble-metal oxides.[18] Many studies using clay-based solid catalysts in biofuel generation have been performed. Recently, some researchers used clay as a heterogamous catalyst to make biofuel manufacturing more cost-effective and environmentally beneficial. It has been observed that the clay-based catalyst may be reused with no loss of activity and can be readily separated from the primary product.

Montmorillonite (MMT, hydrated aluminum silicate) clay has two tetrahedral sheets of silica sand with a central octahedral sheet of alumina (T−O−T) and, owing to the isomorphs' ionic substitutions in the T−O−T structure surface, has net structural negative charge, making it able to adsorb various positively charged species.[19] Clays like MMT are used as appealing materials for various catalytic cracking processes due to their green nature, low cost, non-toxicity, availability, mechanical stability, layered structure, and large surface area.[20,21] The activation of clays using ball milling has been documented in the literature.[22] The application of these green chemistry techniques such as ball milling, for clay, can result in atom size decrease and mechanical activation of the treated clay, which can increase their activity while avoiding excessive calcination temperatures.[23] It also has minimal energy needs and low processing temperatures, which reduces costs and enhances the eco-friendly nature of prepared materials.[24] Researchers are now working on the design and synthesis of novel compounds with more activity that are composed of numerous components named composites and are known as nanocomposites if the particle size of one or more of the components is on the nanoscale.[25]

Chitosan is a D-glucosamine and *N*-acetyl-D-glucosamine copolymer.[25,26] Because of the amino and hydroxyl groups present, which can operate as active sites, chitosan is a very promising material for various applications.[27] Its characteristics are mostly influenced by the amine group's acid−base characteristics.[28] Based on the abovementioned concerns, the primary purpose of this research was to prepare a purified activated montmorillonite (PAMMT) sample and PAMMT-chitosan (PAMMT-CH) nanocomposite, and the mentioned cost-effective materials were utilized for Biojet fuel production via catalytic cracking of waste cooking oil for the first time.

Regarding the published studies on the production of biofuel, the main product that was reported is biodiesel. That was attributed to the low selectivity of these catalysts as the prepared biofuel was the higher-molecular-weight molecules (biodiesel). This manuscript comprises the modification of raw clay with an organic biopolymer with high selectivity toward the production of biojet rather than the most known pathways for preparing catalysts used during pyrolysis of triglycerides, which produced mainly biodiesel. The prepared materials were characterized by FTIR, XRD, S_{BET}, and TEM. Additionally, the synthesized catalysts showed high alkane selectivity and low selectivity toward the production of aromatic hydrocarbon. The reaction pathway of jet biofuel production from waste cooking oils was discussed.

MATERIALS AND METHODS

Materials. Deionized water was used for preparing all solutions. The reagents and chemicals in the experimental study were analytical grade and were used without purification. Chitosan (2×10^3 Da, deacetylation degree = 94%) was obtained from Fluke. Hydrochloric acid (37%), hydrogen peroxide, acetic acid, and sodium hydroxide (98%) were obtained from Merck Chemical Co. Montmorillonite clay was collected from the Western Desert, Egypt, ball-milled, and used after purification and activation. Waste cooking oil was collected from the home's daily use.

Preparation of Treated Montmorillonite Clay. Egyptian raw montmorillonite (MMT) clay was ball-milled using the documented methodology.[29] MMT was dried at 105 °C till a constant weight was obtained; then, 25 g of MMT was milled at 250 rpm for 45 min (FRITSCH, Pulverisette Ball Mill, zirconium-oxide balls) in a 500 mL zirconium oxide vessel at 50 Hz. The resulting sample was purified via treatment with hydrogen peroxide (30%) and distilled water under stirring at 650 rpm for 3 h at 70 °C[30] and left to precipitate. After that, the precipitate was washed by deionized water several times and centrifuged at 2000 rpm for 5 min followed by activation using 5% HCl solution under stirring at 650 rpm for 3 h at 50 °C. Subsequently, the suspension was centrifuged at 2000 rpm for 5 min and the obtained clay was washed repeatedly by deionized water. The precipitate was finally muffled and calcined in air at 400 °C for 2 h and labeled as (PAMMT).

Preparation of the Treated Montmorillonite-Chitosan Nanocomposite (PAMMT-CH). The PAMMT-CH nanocomposite was prepared in a weight ratio of (1:1) by dispersing 3.5 g of PAMMT in distilled water (30 mL) under sonication for 15 min followed by stirring at 750 rpm for 90 min (solution ***A***). A solution of chitosan was prepared by swelling 3.5 g of chitosan in 100 mL of acetic acid solution (2% by weight) (solution ***B***). Then, solution ***A*** was added to solution ***B***, mixed

https://doi.org/10.1021/acsomega.1c06518
ACS Omega 2022, 7, 4585−4594

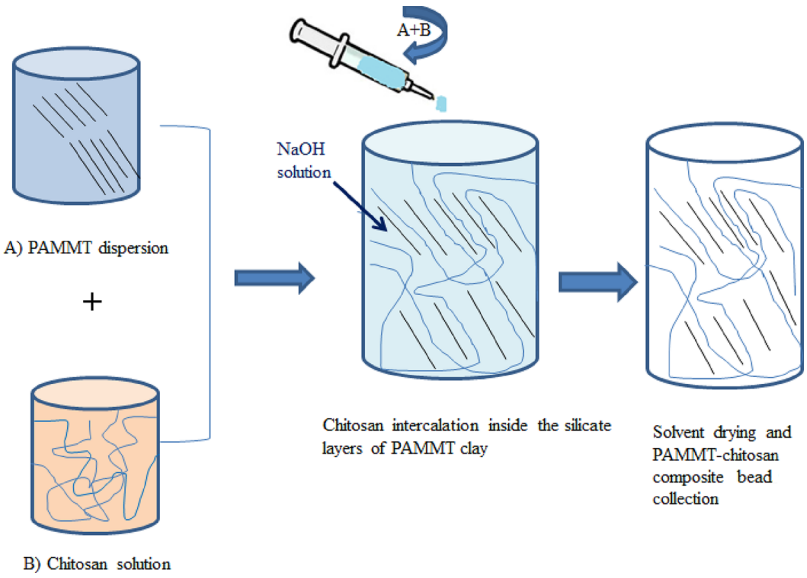

Figure 1. Preparation of the PAMMT-chitosan nanocomposite.

under stirring at 750 rpm for 2 h, and agitated at 70 °C. The resultant mixture was injected gently into sodium hydroxide solution (5 mM) using a syringe to precipitate PAMMT-CH nanocomposite beads. The formed beads were left to precipitate by decantation, washed by warm distilled water to eliminate Na^+ ions, and finally collected by centrifugation.[31] The produced PAMMT-CH nanocomposite was dried at 95 °C for 4 h, as illustrated in Figure 1.

Catalyst Characterization. X-ray diffraction (XRD) patterns of PAMMT and PAMMT-CH nanocomposites were assessed by a PAN-atypical (Empyrean) X-beam diffract meter with Cu Kα radiation (λ = 0.154 cm^{-1}) at 40 kV, 35 mA, scan angle of 20−70°, and ramping of 2°. Transmission electron microscopy (TEM) images of PAMMT and PAMMT-CH nanocomposites on Cu grids were obtained using a JEM-200CX, JEOL-2100 microscope (Japan) worked at 200 kV. A Bruker (Vertex 70 FTIR) spectrometer used to accomplish FTIR investigation of PAMMT and PAMMT-CH nanocomposites at 4000−400 cm^{-1} using a KBr pressed plate. Thermal stabilities of PAMMT and PAMMT-CH nanocomposites were estimated from the thermogravimetric analysis (TGA) as a function of their decomposition at 30−900 °C under a ramping rate of 10 °C/min using a TGA 851e/LF/1100 analyzer utilizing an inert transporter gas (flow rate: 60 mL/min). The surface areas of PAMMT clay and PAMMT-CH composite catalysts were evaluated using the Brunauer−Emmett−Teller (BET) method (Model Autosorb-IQ MP). The surface area, total pore volume, and average pore diameter were determined from the amount of N_2 adsorbed at P/P_0 = 0.1−1.

Catalytic Pyrolysis of Waste Cooking Oil. The catalytic pyrolysis process was carried out at a temperature range of 200−400 °C in a split-type tubular semi-batch reactor using a percentage amount of 0.1−1% of catalyst (PAMMT clay and PAMMT-CH nanocomposite) relative to the used WCO. An electric furnace was used to heat the reactor externally to achieve final temperatures of 200, 250, 300, 350, and 400 °C and kept under the isothermal condition for different periods of 60−120 min. The split-type tubular semi-batch reactor consisted of a three-necked flask equipped with a nitrogen inlet (inert gas) at a flow of 5 mL/min, a thermocouple to contort the temperature, and a condenser.[32] The obtained biofuel was settled in a separating funnel to separate the produced water and then centrifuged to remove any contaminants or dispersed particulates. Finally, the obtained products were categorized as biofuel, water, and solid particulates. The used catalysts were collected for regeneration, washed with ethanol and benzene, and then muffle-activated at 500 °C for 2 h. The yield (%) of the catalytic cracking process was calculated (eq 1):[33]

$$\text{yield of biofuel(mass\%)} = \frac{\text{mass of biofuel collected}}{\text{mass of feed}} \times 100\% \quad (1)$$

RESULTS AND DISCUSSION

Structural Analysis. *FTIR Spectroscopy.* FTIR spectra of PAMMT and PAMMT-CH nanocomposites are displayed in Figure 2. For PAMMT, the strong bands at 1103 and 1030

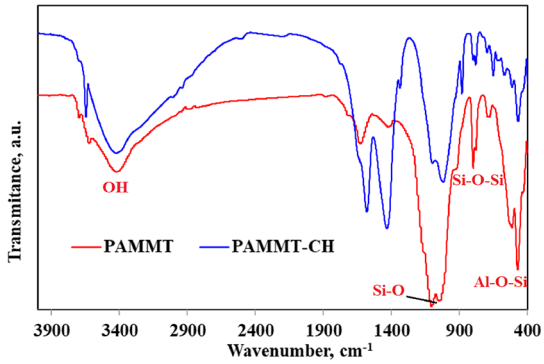

Figure 2. FTIR spectra of PAMMT and PAMMT-CH nanocomposites.

cm^{-1} are due to the out-of-plane and in-plane stretching vibrations of Si−O bonds in the $(SiO)_4$-tetrahedra and absorption bands at 530, 798, and 471 cm^{-1} were assigned to the layered Al−O−Si and Si−O−Si network vibrations.[34] Two broad bands at 3420 and 1625 cm^{-1} were ascribed to OH elongation mode and OH distortion of water molecules,

https://doi.org/10.1021/acsomega.1c06518
ACS Omega 2022, 7, 4585−4594

respectively.[35−37] The band at 3619 cm^{-1} was ascribed to the OH stretching vibrations of Al−OH and Si−OH groups of montmorillonite clay.[3,38] The hydrous nature of the clay material and the presence of hydroxyl linkage are proven by the presence of bands at 3619 and 1625 cm^{-1}.[39] Moreover, the absorption bands at 1031−1038 cm^{-1}, the doublet at 780−798 cm^{-1}, and the band at 920 cm^{-1} can indicate the possible interference of quartz and kaolinite impurities in the MMT sample. The PAMMT-CH nanocomposite catalyst represented the existence of PAMMT clay bands with some changes, besides the appearance of some new bands, shown in Figure 2.

A new strong vibrational band has appeared at 881 cm^{-1} due to the glucosidal structure of chitosan. Shifting of stretching vibrations at 471, 501, 1103, 1030, and 3420 cm^{-1} related to PAMMT to bands at 467, 512, 1155, 1018, and 3417 cm^{-1} for the PAMMT-CH nanocomposite catalyst has been ascribed to the involvement of their bonds in the nanocomposite bead formation. The appearance of the new bands at 1579, 1425, and 1336 cm^{-1} were assigned to the stretching vibrations and symmetrical deformation modes of chitosan after the introduction of $-NH_2$, aliphatic CH_2, and CH_3 to the active functional groups of PAMMT clay. The disappearance of OH bands corresponding to Al−OH and Si−OH at 3619 cm^{-1} in PAMMT endorses the variation of the PAMMT framework to the nanocomposite form. Finally, the observation of a new broadband centered at 3645 cm^{-1}may be assigned to the formation of new hydrogen bonds between the formed PAMMT-CH nanocomposite. The results of FTIR spectra revealed a successful conversion of PAMMT into the PAMMT-CH nanocomposite.

XRD Diffraction Patterns. X-ray diffraction patterns of PAMMT and PAMMT-CH nanocomposite catalysts are depicted in Figure 3. Several diffraction patterns characterized

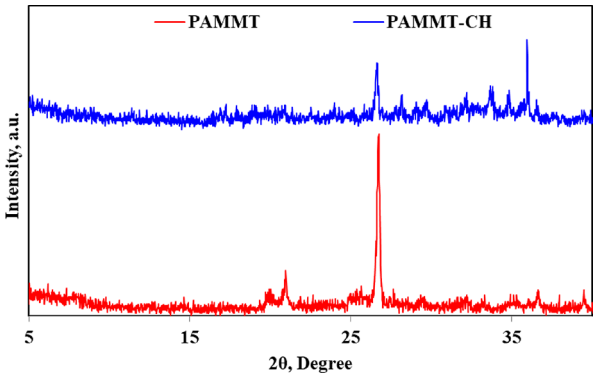

Figure 3. XRD of PAMMT and PAMMT-CH nanocomposites.

the montmorillonite framework at 2θ = 19.8, 26.73, and 35.1° referred to the basal planes of d100, d103, and d006, respectively.[40] The appearance of XRD diffraction patterns at 2θ = 20.9, 35.1, 36.6, and 39.5° associated with PAMMT patterns indicates the presence of impurities such as kaolinite[41] in the MMT clay. The PAMMT-CH nanocomposite diffractogram demonstrates obvious changes in XRD patterns compared to PAMMT clay, which declares the efficient interaction of PAMMT and chitosan. The new two patterns at 2θ = 34.8 and 35.9°may be due to the separation of Al−OH groups from the MMT framework. The patterns of the PAMMT-CH nanocomposite do not have any characteristic pattern related to chitosan, which indicates the intercalation of chitosan inside the silicate layers of the PAMMT framework via cationic exchange during its solubility followed by reprecipitation.[42] Another possible reason for the disappearance of the diffraction patterns of chitosan is the overlapping between the characteristic peak of chitosan, at 2θ = 20.14°, and the characteristics peak of PAMMT.[43] The facile miscibility of chitosan and PAMMT in the acidic medium can be ascribed to the accessibility of a large active hydroxyl and protonated amino groups (−OH and $-NH_3^+$), resulting in its easier intercalation inside the silicate layers by the cationic exchange. The reduction of the pattern intensities recorded in the pristine PAMMT clay of the d103 basal plane at 26.73° may indicate the variation of the crystallinity during the nanocomposite formation.[44] It was reported that the shifting of MMT reflection patterns to the left side angle for the chitosan-MMT nanocomposite could be referred to as the intercalated nanostructure. Also, the intensity of the patterns decreased and the broadening of peaks increased due to the existence of jumbled intercalated or exfoliated structures.[45] The average crystallite sizes (D) of PAMMT and PAMMT-CH catalysts were calculated by applying Scherer's formula and were found at 32.62 and 21.39 nm, respectively.

TEM Microscopy. TEM analysis is the corresponding technique to XRD, which characterizes the nanocomposite structures of PAMMT-CH. For this reason, the obtained XRD data was supported by TEM micrographs. Figure 4a,b shows TEM images of PAMMT and PAMMT-CH nanocomposites. Figure 4a shows the interlayer structures of the clay, while Figure 4b the dark platelets characterize PAMMT, while the gray base represents the uniformly dispersed chitosan biopolymer inside the intercalated silicate layers of PAMMT. Silicate layers of PAMMT are completely and regularly distributed inside the matrix, and the multilayer morphology between silicate layers vanishes in the exfoliated nanocomposite structures. Also, the multilayer morphology is conserved in the intercalated nanocomposite structures. So, intercalated nanocomposite structures can form aggregates and show black aggregates in TEM micrographs. It can be established from TEM micrographs that there are both intercalated and exfoliated nanocomposite structures in the synthesized nanocomposite.[46] Due to the transmittance differences between the composite surface and composite center, it was observed that a layer appeared at the surface of the composite, denoting the PAMMT as the coat onto the cross-linked chitosan inside and illustrating the solid PAMMT layer of the composite.[47] Thereby, TEM findings agree with FTIR and XRD results.

Adsorption−Desorption Isotherms. The obtained adsorption−desorption isotherms of N_2 on surfaces of PAMMT and PAMMT-CH catalysts are represented in Figure 5. The PAMMT catalyst shows type-IV isotherm[4] with type H3-hysteresis loop that characterizes the non-uniform mesoporous solids consisting of aggregated particles of plate-like shapes, giving rise to slit-shaped pores.[48] These pores may result from the exchangeable cations and impurities' removal from the MMT clay lattice following its purification and HCl attack. This result confirmed the isotherm for the layered clay material, possibly due to the multilayer formation and capillary condensation in mesopores (P_D = 2−50 nm).[49] PAMMT hysteresis extends to a very low pressure (P/P_0) range of 0.25−1.0, which may arise from the irreversible uptake of N_2 in the narrowed channels.[50] After the formation of the PAMMT-CH nanocomposite, a type-IV isotherm has been observed, with

https://doi.org/10.1021/acsomega.1c06518
ACS Omega 2022, 7, 4585−4594

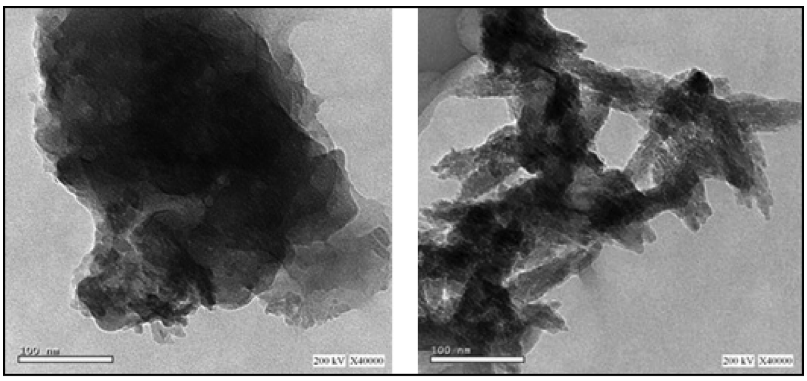

(a) (b)

Figure 4. TEM images of (a) PAMMT and (b) PAMMT-CH nanocomposites.

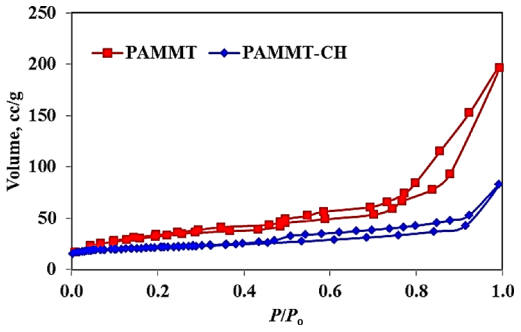

Figure 5. Nitrogen adsorption−desorption isotherm of PAMMT and PAMMT-CH catalysts.

some modification in the H3-hysteresis loop, which extended to a higher P/P_0 regime of 0.45−1.0 (Figure 5). The change reflects the difference like the porous system of the PAMMT-CH nanocomposite compared with that of PAMMT, which could occur due to the electrostatic interaction between the protonated amine groups (NH_3^+) of chitosan and negatively charged sites of PAMMT. Furthermore, a high relative N_2 uptake has been observed, which was associated with a second capillary condensation of N_2. Table 1 summarizes the surface data extracted from the adsorption isotherms.

Table 1. Surface Characteristics of the Synthesized Catalysts

sample	S_{BET}, m^2/g	pore volume, cc/g	pore diameter, nm	references
PAMMT	29.68	0.112	4.349	current study
PAMMT-CH	19.83	0.038	3.561	
Na^+-MMT	46		16.9	51
chi-MMT	23		14.2	
MMT	279	0.455	4.968	52
chitosan/MMT	29.015	0.0448	2.630	

According to Table 1, the PAMMT-CH nanocomposite catalyst exhibited lower S_{BET} (m^2/g), total pore radius (nm), and pore volume (cc/g) values than the data calculated for the PAMMT catalyst. The decrease in the surface area of the PAMMT-CH nanocomposite was attributed to the compact packing of the chitosan molecules in the interlayer space of PAMMT molecules, resulting in pore blocking, which inhibits the passage of N_2.[51,52] The average pore diameter of PAMMT-CH was 3.561 nm compared to 4.349 nm of PAMMT. That can be ascribed to the high dispersion and interaction of chitosan biopolymer particles in the interlayer's framework and the surface of PAMMT, which change the geometry of the nanocomposite pore ranges (Figure 5).

Thermogravimetric Analysis. Thermogravimetric analysis of PAMMT and PAMMT-CH nanocomposites is represented in Figure 6. The thermograms of PAMMT and

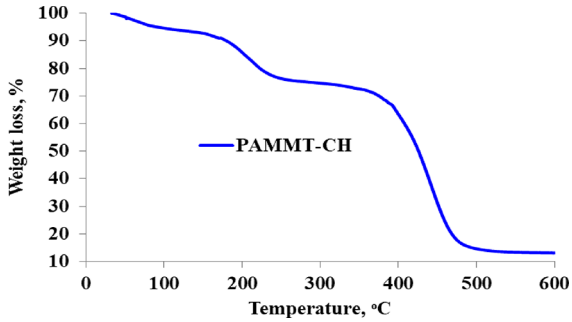

Figure 6. Thermogravimetric analysis of PAMMT and PAMMT-CH nanocomposites.

PAMMT-CH consisted of three main characteristic regions. At 25−140 °C, the percent weight loss is very low at 8%, which represents the evaporation of the adsorbed water molecules at the different catalysts interfaces.[53] The thermogram of PAMMT had two characteristic regions, that at 115−250 °C represents the breakdown of the hydrogen bonds between the clay interlayers, while the sudden decomposition that occurred at 250−340 °C represented the decomposition of the clay structure into silicate.[54] In the PAMMT-CH nanocomposite, it is clear that there is a steeper decrease in the weight loss to about 80% at 140−212 °C, indicating the breakdown of the hydrogen bonds between the hydroxyl and amino groups of the chitosan segments and MMT clay layers.[55] A highly thermal stable area can be observed at the 215−400 °C range. A further increase in the temperature to 400−480 °C causes a high decrease in the weight %, indicating the decomposition of the PAMMT-CH nanostructure framework, and finally, a complete decomposition has occurred at 500 °C. The results of the thermogravimetric study profiled the stability of the prepared PAMMT-CH nanocomposite at the elevated temperature, which was applied in the catalytic pyrolysis process.

Fuel Properties of Biofuel. Table 2 represents the physical and fuel properties of the obtained biofuels from the catalytic pyrolysis process of waste cooking oil using PAMMT

https://doi.org/10.1021/acsomega.1c06518
ACS Omega 2022, 7, 4585−4594

Table 2. Characteristic Properties of WCO Used in Catalytic Cracking

properties	WCO
viscosity at (100 °C mm^2/s)	48.7
density at 15 °C (kg/m^3)	927
acidity (mg KOH/g)	2.85
water content (ppm)	480
iodine value (mg I_2/100 g oil)	121
saponification value (mg KOH/g)	191

and PAMMT-CH nanocomposite catalysts. It is clear from the properties that the PAMMT catalyst produces heavier hydrocarbon, according to the values of density, viscosity, pour point, flash point, and gum content. On the other hand, the characteristics of the biofuel produced from the catalyzed pyrolysis of WCO using the PAMMT-CH catalyst showed lower viscosity, density, pour point, and higher flash point values.

Inspecting the characteristics of biofuel obtained from the catalytic pyrolysis of WCO using PAMMT (Table 3) revealed that this type of fuel is comparable to biodiesel. That was obvious clearly from the viscosity, density, and flash point values.

The density of the obtained biofuel was 0.8568, which was in the agreed record of the ASTM D 6751 standards (0.860−0.900 g/cm^3).[56] On the other hand, inspecting the value of the viscosity (4.93 mm^2/s) was pointed an acceptable value (1.6 to 7.0 mm^2/s). The approved viscosity of the fuel prevents engine defects during its supply in the engine chamber. The acceptable values of the obtained biodiesel regarding the viscosity and density were following the published data. Similarly, Table 3 reveals the pour point of the obtained biodiesel at −9 °C, which is located within the range of ASTM D 6751 values (−5 to 15 °C). This lessening compared to the used WCO reveals the decline in the length of the hydrocarbon in the obtained biodiesel.[57] Volatility has affected the flash point of biodiesel. The obtained value of flash point of the obtained biodiesel was 55 °C, which can be considered a suitable value for diesel engines (Table 3). Gum formation in diesel engines can be considered a serious problem during injection and ignition due to the plugging of valves and joints. The acceptable value of gum in biodiesel according to the ASTM D-6751 specification is 7 ppm max, while the obtained gum concentration was 4.7 ppm. The obtained data agreed with both ASTM D 6751 specifications and the published values of biodiesel produced using waste cooking oil.[14]

On the other hand, the properties of the obtained biojet using the PAMMT-CH catalyst were in the acceptable values of ASTM D-1655 records.[6] The density of the biojet was 0.8037 g/cm^3 that is located at 0.775−0.840 g/m^3, and the viscosity was 3.45 mm^2/s, which were in the ASTM D-1655 range. According to the measured fuel characterizations of the produced biojet, pour point, flash point, and gum content were −54 °C, 36 °C, and 1.6 ppm, respectively, which were within the accepted range of standard specifications (−50 °C min, 38 °C min, and 7 ppm max); these values agreed with those of commercial-grade jet A-1 petroleum fuel ASTM D1655 and followed the published values of biojet produced from waste cooking oil[58,59] (Table 3). The explanation for this might be that during the reactions, longer hydrocarbon molecules of WCO were broken into smaller/lighter fractions with oxygen elimination, which were produced during the chemical interactions of the PAMMT-CH catalyst by WCO.[57,60]

Effect of Reaction Parameters on Catalytic Pyrolysis of WCO. The lab-scale catalytic pyrolysis of WCO in a semi-batch reactor is discussed in this section. The yields of the obtained biofuels were highly dependent on the pyrolysis temperature, time, heating rate, and used catalyst concentration.

Effect of Used Catalyst Amount. In catalytic pyrolysis processes, catalyst selection is an important factor due to its role in product yield and component selectivity for the obtained biofuel. The effectiveness of a catalyst for catalytic pyrolysis has been determined by its active site, pore volume, pore size, and surface area. The effect of the used catalyst amount on the biofuel yield has been investigated at a catalyst amount of 0.1−1.0 wt %. Figure 7 shows the effect of PAMMT and PAMMT-CH nanocomposite catalyst amounts on the percentage conversion of WCO into biofuel. The obtained biofuel yield depends on the amounts of catalysts used during the catalytic pyrolysis process. In the case of the PAMMT catalyst, the obtained jet fuel yields 71% at the highest ratio

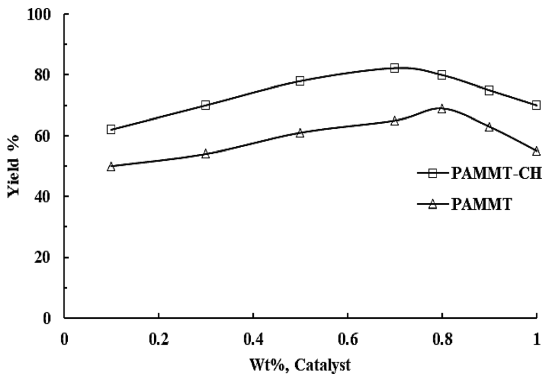

Figure 7. Influence of catalyst amount on the yield % of the obtained biofuel using (triangles with strikethrough) PAMMT and (squares with strikethrough) PAMMT-CH nanocomposite catalysts.

Table 3. Characteristic Properties of Biofuels from Catalytic Cracking of WCO Using PAMMT, PAMMT-CH Catalyst, and ASTM Specification of Fuels

					published data	
property	biofuel/ PAMMT	biofuel/PAMMT-CH	ASTM D1655 jet A-1[6]	ASTM D 6751 biodiesel[56]	WCO biojet[58,59]	WCO biofuel[14]
density at 15 °C (g/m^3)	0.8568	0.8037	0.775−0.840	0.860−0.900	0.759	0.8992
viscosity at 40 °C (mm^2/s)	4.93	3.45	3.27−4.12	1.6−7.0	3.8	6.11
pour point (°C)	−9	−54	−50 (min)	−5 to 15	−54.3	−12
flash point (°C)	55	36	38 (min)	52 (min)	42	45
gum content (ppm)	4.7	1.6	7 (max)	7 (max)	<0.3	0.06

https://doi.org/10.1021/acsomega.1c06518
ACS Omega 2022, 7, 4585−4594

used (1%). Meanwhile, the catalytic cracking process in the presence of the PAMMT-CH nanocomposite produced comparatively higher jet fuel that reached 90%. It is also clear that the catalyst ratio of 0.7% of PAMMT-CH is the optimum amount for obtaining jet fuel at 90%. A deep insight in Figure 7 shows two characteristic regions for producing the jet fuel. The first is at a gradual increase in the catalyst amount to 0.7 wt %, which is characterized by a gradual increase in the jet fuel yield. Second, a further increase in the amount of the catalyst has a depressing effect on the percentage of jet fuel yield. The rate of the catalytic pyrolysis process was gradually increased by increasing the catalyst ratio, which can be attributed to the presence of the active sites and their concentration in the used catalyst. The percentage of catalytic pyrolysis is proportional to the number of active sites on the catalyst, so a higher catalyst ratio provides more active sites for the reaction. The yield of biofuel has been reduced by increasing the catalyst ratio. This could be attributed to the increased catalyst amount, which resulted in aggregation of catalyst active sites,[61] which lowers its catalytic activity. A higher catalyst ratio increased the progress of the catalytic pyrolysis process as a result from the chromatographic study of the obtained biofuels using PAMMT-CH, which leads to a higher extent of cracking for the hydrocarbon chains and consequently shorter hydrocarbon chains produced (C_4–C_6). Confirmation of this observation has been proven from the coke produced during the cracking process and its deposition on the catalyst surface. These results are analogous to the results reported in the literature.[62]

Effect of Temperature. Temperature is a critical factor in the catalytic pyrolysis of WCO. Experiments have been performed at various temperatures (200, 250, 300, 350, and 400 °C) to evaluate the effect of temperature on the production of the biofuel production process. Figure 8 depicts

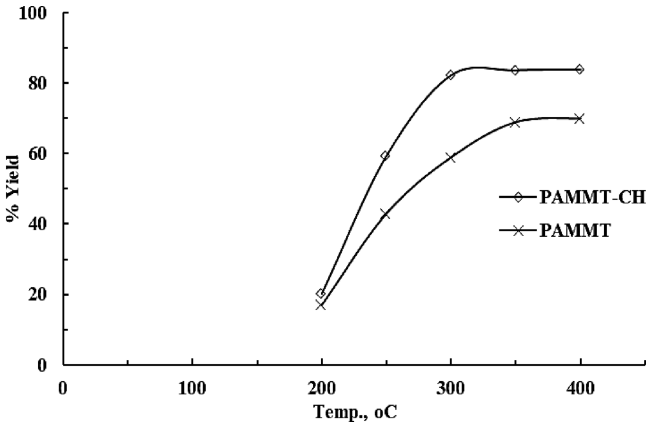

Figure 8. Influence of temperature on the yield % of the obtained biofuel using: (crosses) PAMMT and (diamonds) PAMMT-CH nanocomposite catalysts.

the effect of reaction temperature on biofuel yield. It has been discovered in Figure 8 that the pyrolysis temperature represents an important key parameter for waste cooking oil. To investigate the effect of temperature on the yield of the biofuel production process, several experiments have been carried out at different temperatures, viz., 200, 250, 300, 350, and 400 °C. From Figure 8, it was discovered that the pyrolysis temperature had an important influence on biofuel yield.[63] The yield of biofuel was gradually increased from 20% at 200 °C to 82.33% at 300 °C. However, increasing the temperature did not significantly increase the quality of yield conversion. The temperature study revealed that PAMMT-CH yielded 82.3% at 300 °C, while PAMMT yielded 59% at similar temperatures. Furthermore, increasing the temperature to 400 °C had no significant increase in the yield percent of the obtained jet fuel.

Effect of Process Time. The processing time represents the time of the catalytic pyrolysis reaction. The biofuel yield of catalytic pyrolysis of WCO is greatly influenced by the time of the reaction. The influence of process time on the biofuel yield has been investigated in this study during a time range of 60, 120, 180, 240, and 300 min. The yield of biofuel has been increased from 32.4 to 82.3% as the processing time increased from 60 to 120 min. Increasing the reaction time to 300 min had a slight decrease in biofuel yield (Figure 9). This could be

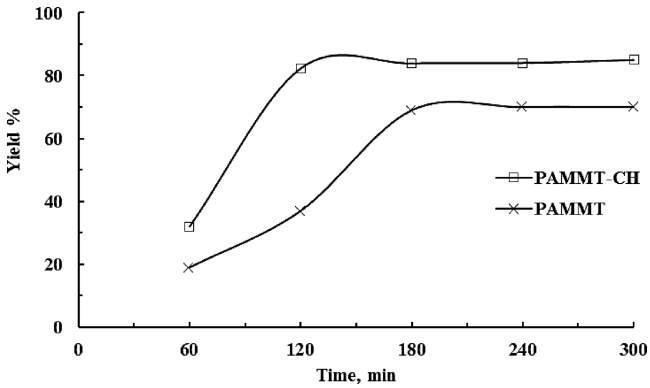

Figure 9. Influence of reaction time on the yield % of the obtained biofuel using (crosses) PAMMT and (squares) PAMMT-CH nanocomposite catalysts.

ascribed to the prolonged contact time of biofuel with the catalyst, which resulted in the formation of side products.[64] The current study agreed with a previous study on waste cooking oil published in the literature.[57] However, as shown in Figure 9, the time required to complete the cracking was 120 min. As a result, an optimum process time was found to be 120 min for obtaining the highest biofuel yield.

Mechanism of Catalytic Cracking. X-ray fluorescence spectroscopy showed the elemental and chemical compositions of MMT clay used in the modification of the catalyst as follows: Al_2O_3 (18.79), MgO (6.44), Fe_2O_3 (2.8), and CaO (3.98). The type of metal salts present in the used MMT plays a vital role in their tendency toward the activation of the catalytic cracking process and the obtained products.[65] It is clear that the most abundant metals present were Al, Mg, Fe, and Ca metal ions.

The mechanism of catalytic cracking in the presence of MMT is the electron transfer mechanism. This mechanism involves the adsorption of triglyceride molecules on the catalyst surface via interaction by the unsaturation sites presented in the fatty acid alkyl chains of the triglyceride molecules.[32] The electron transfer mechanism can be promoted due to the presence of Fe_2O_3, where the redox reaction of Fe^{+3} to Fe^{+2} is the predominant reaction. The redox steps of Fe can be illustrated in the following equations:

$$Fe^{+3} + TGS \rightarrow Fe^{+2} + TGS \quad (2)$$

$$Fe^{+2} \rightarrow Fe^{+3} + \bar{e} \quad (3)$$

https://doi.org/10.1021/acsomega.1c06518
ACS Omega 2022, 7, 4585−4594

$$TGS + \bar{e} \rightarrow TGS \quad (4)$$

The generation of the free radicals occurred due to the cracking of the double bonds in the fatty acid chains of the triglyceride's molecules.[66] According to the literature results,[66] the free radical cracking of the triglyceride molecules during the redox reaction process produces a high yield abundance of C_8−C_{18} hydrocarbon chains with a saturated alkane ratio in a range of 30−32% and an alkene ratio of 37% (Figure 10).

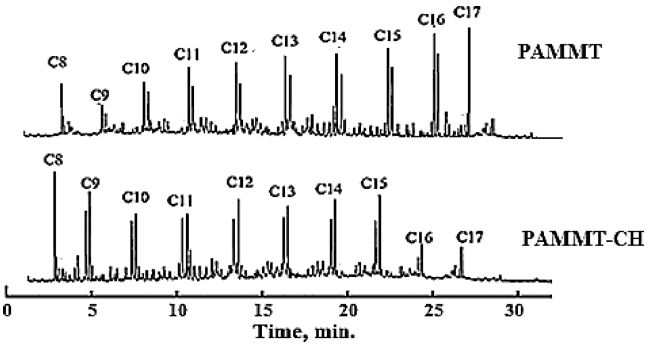

Figure 10. GC/MS diagram of the obtained biofuel from catalytic cracking of WCO using PAMMT and PAMMT-CH catalysts.

The chemical composition of the used oil as obtained from GC−MS (Figure 10) showed high unsaturated fatty acid chain abundance, which was further confirmed by the high iodine value of the used oil (105 g I_2/100 mL oil). The carbon distributions of the obtained biofuel from the catalytic cracking of waste cooking oil using PAMMT and PAMMT-CH catalysts were determined from GC−MS spectroscopy (Figure 10). The carbon distribution of the obtained hydrocarbon chains was found to be at 60% for C_{12}−C_{17} hydrocarbons. In the case of PAMMT-CH, it is clear that the obtained hydrocarbon fractions of C_8−C_{12} were 75% of the total yield, while the hydrocarbon fractions of C_{13}−C_{17} were 20% of the total yield. The higher short-chain hydrocarbons were produced due to the high activity reported for the redox system of Fe^{2+} to Fe^{3+}. The higher reactivity of the prepared catalyst (PAMMT-CH) can be attributed to three main reasons. The first is the high catalyst selectivity, which originated from the regular pore diameter and pore size of the framework. The smaller pore diameter and volume controlled the catalytic reaction of the triglyceride, which produces a homologous type of product including under the category of biojet.[67] It was reported that a smaller pore volume has a controlling action on the type of the products. Larger pore volumes and diameters resulted in diverse types of compounds,[68] while the opposite is correct. First, the presence of chitosan in the framework of the prepared catalyst has two functions. Second, the hydrophobic character of chitosan due to the presence of $-CH_2$ groups increases the interaction between the triglyceride molecules and MMT.[69] Finally, the polar groups of chitosan can interact with the unsaturated centers of triglycerides, which increased the double bond polarization and consequently the generation of the free radicals during the interaction with Fe ions.

CONCLUSIONS

Montmorillonite clay was chemically activated and modified by chitosan to obtain modified nanocomposite catalysts efficient for catalytic pyrolysis of waste cooking oil into highly efficient biojet fuel. The optimum conditions for producing the biojet were a 0.7% catalyst ratio for 120 min at 300 °C. The obtained biojet was comparable to the standard limits of ASTM specifications. The catalysts were tested for their performances using different amounts (0.1−1% by weight) at a temperature assortment of 200−400 °C during a time range of 60−300 min. Fractional distillation is used to separate final products from various reaction conditions. The characteristic (physical and fuel) properties of the resulting biofuels were profiled by quantifying their densities, viscosities, specific gravities, pour points, flash and fire points, cetane numbers, carbon and ash residues, and sulfur contents. The optimum conditions of yield product were 300 and 400 °C, catalyst weights of 0.7 and 0.8% w/v, and reaction times of 120 and 180 min concerning (PAMMT) and (PAMMT-CH) nanocomposite, respectively.

AUTHOR INFORMATION

Corresponding Authors

Nabel A. Negm − *Egyptian Petroleum Research Institute, Cairo 11727, Egypt*; Email: nabelnegm@hotmail.com

Eslam A. Mohamed − *Egyptian Petroleum Research Institute, Cairo 11727, Egypt*; orcid.org/0000-0002-5787-5882; Email: eslamazmy60@yahoo.com

Authors

Hanan A. Ahmed − *Egyptian Petroleum Research Institute, Cairo 11727, Egypt*

Amal A. Altalhi − *Department of Chemistry, College of Science, Taif University, Taif 21944, Saudi Arabia*

Sameh A. Elbanna − *Egyptian Petroleum Research Institute, Cairo 11727, Egypt*

Hend A. El-Saied − *Egyptian Petroleum Research Institute, Cairo 11727, Egypt*

Ahmed A. Farag − *Egyptian Petroleum Research Institute, Cairo 11727, Egypt*

Complete contact information is available at: https://pubs.acs.org/10.1021/acsomega.1c06518

Notes

The authors declare no competing financial interest.

ACKNOWLEDGMENTS

The author would like to thank Taif University Researcher supporting project number (TURP-2020/243), Taif University, Taif, Saudi Arabia. Also, the author would like to thank Prof. Dr. Nabel A. Negm and Prof. Dr. Salwa M. Morsy and the Egyptian Petroleum Research Institute (EPRI).

REFERENCES

(1) Chen, Y.-K.; Hsieh, C.-H.; Wang, W.-C. The Production of Renewable Aviation Fuel from Waste Cooking Oil. Part II: Catalytic Hydro-Cracking/Isomerization of Hydro-Processed Alkanes into Jet Fuel Range Products. *Renewable Energy* **2020**, *157*, 731−740.

(2) Phasukarratchai, N. Phase Behavior and Biofuel Properties of Waste Cooking Oil-Alcohol-Diesel Blending in Microemulsion Form. *Fuel* **2019**, *243*, 125−132.

(3) Negm, N. A.; Sayed, G. H.; Yehia, F. Z.; Habib, O. I.; Mohamed, E. A. Biodiesel Production from One-Step Heterogeneous Catalyzed Process of Castor Oil and Jatropha Oil Using Novel Sulphonated Phenyl Silane Montmorillonite Catalyst. *J. Mol. Liq.* **2017**, *234*, 157−163.

(4) Negm, N. A.; Rabie, A. M.; Mohammed, E. A. Molecular Interaction of Heterogeneous Catalyst in Catalytic Cracking Process of Vegetable Oils: Chromatographic and Biofuel Performance Investigation. *Appl. Catal. B Environ.* **2018**, *239*, 36−45.

(5) Barbera, E.; Naurzaliyev, R.; Asiedu, A.; Bertucco, A.; Resurreccion, E. P.; Kumar, S. Techno-Economic Analysis and Life-Cycle Assessment of Jet Fuels Production from Waste Cooking Oil via in Situ Catalytic Transfer Hydrogenation. *Renewable Energy* **2020**, *160*, 428−449.
(6) Goh, B. H. H.; Chong, C. T.; Ge, Y.; Ong, H. C.; Ng, J.-H.; Tian, B.; Ashokkumar, V.; Lim, S.; Seljak, T.; Józsa, V. Progress in Utilisation of Waste Cooking Oil for Sustainable Biodiesel and Biojet Fuel Production. *Energy Convers. Manage.* **2020**, *223*, 113296.
(7) Bhikuning, A.; Sugawara, R.; Matsumura, E.; Senda, J. Investigation of Spray Characteristics from Waste Cooking Oil, Bio-Hydro Fined Diesel Oil (BHD)and n-Tridecane in a Constant Volume Chamber. *Case Stud. Therm. Eng.* **2020**, *21*, 100661.
(8) Wang, W.-C.; Tao, L.; Markham, J.; Zhang, Y.; Tan, E.; Batan, L.; Biddy, M.; Wang, W.-C.; Tao, L.; Zhang, Y.; Tan, E.; Warner, E.; Biddy, M. Review of Biojet Fuel Conversion Technologies. National Renewable Energy Laboratory, Technical Report NREL/TP-5100-66291. 2016, No. July, 98.
(9) El-Araby, R.; Abdelkader, E.; El Diwani, G.; Hawash, S. I. Bio-Aviation Fuel via Catalytic Hydrocracking of Waste Cooking Oils. *Bull. Natl. Res. Cent.* **2020**, *44*, 177.
(10) Yang, J.; Xin, Z.; He, Q. (. S.; Corscadden, K.; Niu, H. An Overview on Performance Characteristics of Bio-Jet Fuels. *Fuel* **2019**, *237*, 916−936.
(11) Foo, W. H.; Chia, W. Y.; Tang, D. Y. Y.; Koay, S. S. N.; Lim, S. S.; Chew, K. W. The Conundrum of Waste Cooking Oil: Transforming Hazard into Energy. *J. Hazard. Mater.* **2021**, *417*, 126129.
(12) Gutiérrez-Antonio, C.; Romero-Izquierdo, A. G.; Gómez-Castro, F. I.; Hernández, S. *8 - The Future Trends in the Production of Biojet Fuel*; Gutiérrez-Antonio, C., Romero-Izquierdo, A. G., Gómez-Castro, F. I., Hernández, S. B. T.-P. P. of R. A. F., Eds.; Elsevier, 2021; pp. 241−254. DOI: 10.1016/B978-0-12-819719-6.00008-0.
(13) Negm, N. A.; Sayed, G. H.; Yehia, F. Z.; Dimitry, O. I. H.; Rabie, A. M.; Azmy, E. A. M. Production of Biodiesel Production from Castor Oil Using Modified Montmorillonite Clay. *Egypt. J. Chem.* **2016**, *59*, 1045−1060.
(14) Altalhi, A. A.; Morsy, S. M.; Abou Kana, M. T. H.; Negm, N. A.; Mohamed, E. A. Pyrolytic Conversion of Waste Edible Oil into Biofuel Using Sulphonated Modified Alumina. *Alexandria Eng. J.* **2022**, 4847.
(15) Đặng, T.-H.; Nguyễn, X.-H.; Chou, C.-L.; Chen, B.-H. Preparation of Cancrinite-Type Zeolite from Diatomaceous Earth as Transesterification Catalysts for Biodiesel Production. *Renewable Energy* **2021**, *174*, 347−358.
(16) Yusuff, A. S.; Bhonsle, A. K.; Trivedi, J.; Bangwal, D. P.; Singh, L. P.; Atray, N. Synthesis and Characterization of Coal Fly Ash Supported Zinc Oxide Catalyst for Biodiesel Production Using Used Cooking Oil as Feed. *Renewable Energy* **2021**, *170*, 302−314.
(17) Jaya, N.; Selvan, B. K.; Vennison, S. J. Synthesis of Biodiesel from Pongamia Oil Using Heterogeneous Ion-Exchange Resin Catalyst. *Ecotoxicol. Environ. Saf.* **2015**, *121*, 3−9.
(18) Sadeek, S. A.; Mohammed, E. A.; Shaban, M.; Abou, M. T. H.; Negm, N. A. Synthesis , Characterization and Catalytic Performances of Activated Carbon-Doped Transition Metals during Biofuel Production from Waste Cooking Oils. *J. Mol. Liq.* **2020**, *306*, 112749.
(19) Munir, M.; Ahmad, M.; Rehan, M.; Saeed, M.; Lam, S. S.; Nizami, A. S.; Waseem, A.; Sultana, S.; Zafar, M. Production of High Quality Biodiesel from Novel Non-Edible Raphnus Raphanistrum L. *Seed Oil Using Copper Modified Montmorillonite Clay Catalyst. Environ. Res.* **2021**, *193*, 110398.
(20) Nagendrappa, G. Organic Synthesis Using Clay and Clay-Supported Catalysts. *Appl. Clay Sci.* **2011**, *53*, 106−138.
(21) Rabie, A. M.; Mohammed, E. A.; Negm, N. A. Feasibility of Modified Bentonite as Acidic Heterogeneous Catalyst in Low Temperature Catalytic Cracking Process of Biofuel Production from Nonedible Vegetable Oils. *J. Mol. Liq.* **2018**, *254*, 260−266.
(22) Masindi, V.; Ramakokovhu, M. M. The Performance of Thermally Activated and Vibratory Ball Milled South African Bentonite Clay for the Removal of Chromium Ions from Aqueous Solution. *Mater. Today Proc.* **2021**, *38*, 964−974.
(23) Chatterjee, U.; Butola, B. S.; Joshi, M. High Energy Ball Milling for the Processing of Organo-Montmorillonite in Bulk. *Appl. Clay Sci.* **2017**, *140*, 10−16.
(24) Mangiacapra, P.; Gorrasi, G.; Sorrentino, A.; Vittoria, V. Biodegradable Nanocomposites Obtained by Ball Milling of Pectin and Montmorillonites. *Carbohydr. Polym.* **2006**, *64*, 516−523.
(25) Azmy, E. A. M.; Hashem, H. E.; Mohamed, E. A.; Negm, N. A. Synthesis, Characterization, Swelling and Antimicrobial Efficacies of Chemically Modified Chitosan Biopolymer. *J. Mol. Liq.* **2019**, *284*, 748−754.
(26) Negm, N. A.; Abubshait, H. A.; Abubshait, S. A.; Abou Kana, M. T. H.; Mohamed, E. A.; Betiha, M. M. Performance of Chitosan Polymer as Platform during Sensors Fabrication and Sensing Applications. *Int. J. Biol. Macromol.* **2020**, *165*, 402−435.
(27) Negi, H.; Verma, P.; Singh, R. K. A Comprehensive Review on the Applications of Functionalized Chitosan in Petroleum Industry. *Carbohydr. Polym.* **2021**, *266*, 118125.
(28) Allison, C. L.; Lutzke, A.; Reynolds, M. M. Examining the Effect of Common Nitrosating Agents on Chitosan Using a Glucosamine Oligosaccharide Model System. *Carbohydr. Polym.* **2019**, *203*, 285−291.
(29) Yan, Y.; Kuramae, E. E.; De Hollander, M.; Klinkhamer, P. G. L.; Van Veen, J. A. Functional Traits Dominate the Diversity-Related Selection of Bacterial Communities in the Rhizosphere. *ISME J.* **2017**, *11*, 56−66.
(30) Mao, H.; Li, B.; Yue, L.; Wang, L.; Yang, J.; Gao, X. Aluminated Mesoporous Silica-Pillared Montmorillonite as Acidic Catalyst for Catalytic Cracking. *Appl. Clay Sci.* **2011**, *53*, 676−683.
(31) Jafari, H.; Atlasi, Z.; Mahdavinia, G. R.; Hadifar, S.; Sabzi, M. Magnetic κ-Carrageenan/Chitosan/Montmorillonite Nanocomposite Hydrogels with Controlled Sunitinib Release. *Mater. Sci. Eng. C* **2021**, *124*, 112042.
(32) Altalhi, A. A.; Mohammed, E. A.; Morsy, S. S. M.; Negm, N. A.; Farag, A. A. Catalyzed Production of Different Grade Biofuels Using Metal Ions Modified Activated Carbon of Cellulosic Wastes. *Fuel* **2021**, *295*, 120646.
(33) Abnisa, F.; Wan Daud, W. M. A.; Ramalingam, S.; Azemi, M. N. B. M.; Sahu, J. N. Co-Pyrolysis of Palm Shell and Polystyrene Waste Mixtures to Synthesis Liquid Fuel. *Fuel* **2013**, *108*, 311−318.
(34) Negm, N. A.; Sayed, G. H.; Habib, O. I.; Yehia, F. Z.; Mohamed, E. A. Heterogeneous Catalytic Transformation of Vegetable Oils into Biodiesel in One-Step Reaction Using Super Acidic Sulfonated Modified Mica Catalyst. *J. Mol. Liq.* **2017**, *237*, 38−45.
(35) Anwer, K. E.; Farag, A. A.; Mohamed, E. A.; Azmy, E. M.; Sayed, G. H. Corrosion Inhibition Performance and Computational Studies of Pyridine and Pyran Derivatives for API X-65 Steel in 6M H2SO4. *J. Ind. Eng. Chem.* **2021**, 523.
(36) Farag, A. A.; Mohamed, E. A.; Sayed, G. H.; Anwer, K. E. Experimental/Computational Assessments of API Steel in 6 M H2SO4 Medium Containing Novel Pyridine Derivatives as Corrosion Inhibitors. *J. Mol. Liq.* **2021**, *330*, 115705.
(37) Farag, A. A. Applications of Nanomaterials in Corrosion Protection Coatings and Inhibitors. *Corros. Rev.* **2020**, *38*, 67−86.
(38) Abubshait, H. A.; Farag, A. A.; El-Raouf, M. A.; Negm, N. A.; Mohamed, E. A. Graphene Oxide Modified Thiosemicarbazide Nanocomposite as an Effective Eliminator for Heavy Metal Ions. *J. Mol. Liq.* **2021**, 114790.
(39) Altalhi, A. A.; Hashem, H. E.; Negm, N. A.; Mohamed, E. A.; Azmy, E. M. Synthesis, Characterization, Computational Study, and Screening of Novel 1-Phenyl-4-(2-Phenylacetyl)-Thiosemicarbazide Derivatives for Their Antioxidant and Antimicrobial Activities. *J. Mol. Liq.* **2021**, *333*, 115977.
(40) Kumar, A. S. K.; Kalidhasan, S.; Rajesh, V.; Rajesh, N. A Meticulous Study on the Adsorption of Mercury as Tetrachlor-omercurate (II) Anion with Trioctylamine Modified Sodium

https://doi.org/10.1021/acsomega.1c06518
ACS Omega 2022, 7, 4585−4594

Montmorillonite and Its Application to a Coal Fly Ash Sample. *Ind. Eng. Chem. Res.* **2012**, *51*, 11312−11327.
(41) Kłosek-Wawrzyn, E.; Małolepszy, J.; Murzyn, P. Sintering Behavior of Kaolin with Calcite. *Procedia Eng.* **2013**, *57*, 572−582.
(42) Dubois, P.; Rosset, S.; Koster, S.; Stauffer, J.; Mikhaïlov, S.; Dadras, M.; Rooij, N. F. d.; Shea, H. Microactuators Based on Ion Implanted Dielectric Electroactive Polymer (EAP) Membranes. *Sensors Actuators, A Phys.* **2006**, *130−131*, 147−154.
(43) Rhim, J.-W.; Hong, S.-I.; Park, H.-M.; Ng, P. K. W. Preparation and Characterization of Chitosan-Based Nanocomposite Films with Antimicrobial Activity. *J. Agric. Food Chem.* **2006**, *54*, 5814−5822.
(44) Okamoto, K.; Ray, S. S.; Okamoto, M. New Poly(Butylene Succinate)/Layered Silicate Nanocomposites. II. Effect of Organically Modified Layered Silicates on Structure, Properties, Melt Rheology, and Biodegradability. *J. Polym. Sci. Part B Polym. Phys.* **2003**, *41*, 3160−3172.
(45) Bensalem, S.; Hamdi, B.; Confetto, S.; Balard, H.; Calvet, R.; Bensalem, S.; Hamdi, B.; Confetto, S.; Chamayou, A. Characterization of Chitosan / Montmorillonite Bionanocomposites by Inverse Gas Chromatography To Cite This Version : HAL Id : Hal-01619253 Inverse Gas Chromatography. *Colloids Surfaces A Physicochem. Eng. Asp.* **2017**, *516*, 336−344.
(46) Tunç, S.; Duman, O. Preparation and Characterization of Biodegradable Methyl Cellulose/Montmorillonite Nanocomposite Films. *Appl. Clay Sci.* **2010**, *48*, 414−424.
(47) Li, Q.; Mao, Q.; Yang, C.; Zhang, S.; He, G.; Zhang, X.; Zhang, W. Hydrophobic-Modified Montmorillonite Coating onto Cross-linked Chitosan as the Core-Shell Micro-Sorbent for Iodide Adsorptive Removal via Pickering Emulsion Polymerization. *Int. J. Biol. Macromol.* **2019**, *141*, 987−996.
(48) Lertsutthiwong, P.; Noomun, K.; Khunthon, S.; Limpanart, S. Influence of Chitosan Characteristics on the Properties of Biopolymeric Chitosan−Montmorillonite. *Prog. Nat. Sci. Mater. Int.* **2012**, *22*, 502−508.
(49) Shehap, A. M.; Nasr, R. A.; Mahfouz, M. A.; Ismail, A. M. Preparation and Characterizations of High Doping Chitosan/MMT Nanocomposites Films for Removing Iron from Ground Water. *J. Environ. Chem. Eng.* **2021**, *9*, 104700.
(50) Teimouri, A.; Ghanavati Nasab, S.; Habibollahi, S.; Fazel-Najafabadi, M.; Chermahini, A. N. Synthesis and Characterization of a Chitosan/Montmorillonite/ZrO2 Nanocomposite and Its Application as an Adsorbent for Removal of Fluoride. *RSC Adv.* **2015**, *5*, 6771−6781.
(51) Monvisade, P.; Siriphannon, P. Chitosan Intercalated Montmorillonite: Preparation, Characterization and Cationic Dye Adsorption. *Appl. Clay Sci.* **2009**, *42*, 427−431.
(52) Karaca, S.; Önal, E. Ç.; Açışlı, Ö.; Khataee, A. Preparation of Chitosan Modified Montmorillonite Biocomposite for Sonocatalysis of Dyes: Parameters and Degradation Mechanism. *Mater. Chem. Phys.* **2021**, *260*, 124125.
(53) Rodrigues, C.; de Mello, J. M. M.; Dalcanton, F.; Macuvele, D. L. P.; Padoin, N.; Fiori, M. A.; Soares, C.; Riella, H. G. Mechanical, Thermal and Antimicrobial Properties of Chitosan-Based-Nanocomposite with Potential Applications for Food Packaging. *J. Polym. Environ.* **2020**, *28*, 1216−1236.
(54) Ahmad, M. B.; Gharayebi, Y.; Salit, M. S.; Hussein, M. Z.; Shameli, K. Comparison of In Situ Polymerization and Solution-Dispersion Techniques in the Preparation of Polyimide/Montmorillonite (MMT) Nanocomposites. *Int. J. Mol. Sci.* **2011**, *12*, 6040−6050.
(55) Kasirga, Y.; Oral, A.; Caner, C. Preparation and Characterization of Chitosan/Montmorillonite-K10 Nanocomposites Films for Food Packaging Applications. *Polym. Compos.* **2012**, *33*, 1874−1882.
(56) Kipkorir, D.; Nturanabo, F.; Tewo, R.; Rutto, H.; Enweremadu, C. Properties of Waste-Distilled Engine Oil and Biodiesel Ternary Blends. *Heliyon* **2021**, *7*, No. e07858.
(57) Wako, F. M.; Reshad, A. S.; Bhalerao, M. S.; Goud, V. V. Catalytic Cracking of Waste Cooking Oil for Biofuel Production Using Zirconium Oxide Catalyst. *Ind. Crops Prod.* **2018**, *118*, 282−289.
(58) Yıldız, A.; Goldfarb, J. L.; Ceylan, S. Sustainable Hydrocarbon Fuels via "One-Pot" Catalytic Deoxygenation of Waste Cooking Oil Using Inexpensive, Unsupported Metal Oxide Catalysts. *Fuel* **2020**, *263*, 116750.
(59) Buffi, M.; Valera-Medina, A.; Marsh, R.; Pugh, D.; Giles, A.; Runyon, J.; Chiaramonti, D. Emissions Characterization Tests for Hydrotreated Renewable Jet Fuel from Used Cooking Oil and Its Blends. *Appl. Energy* **2017**, *201*, 84−93.
(60) Zhao, L.; Chang, S.; Wang, H.; Zhang, X.; Ou, X.; Wang, B.; Wu, M. Long-Term Projections of Liquid Biofuels in China: Uncertainties and Potential Benefits. *Energy* **2015**, *83*, 37−54.
(61) Zhang, H.; Xiao, R.; Huang, H.; Xiao, G. Comparison of Non-Catalytic and Catalytic Fast Pyrolysis of Corncob in a Fluidized Bed Reactor. *Bioresour. Technol.* **2009**, *100*, 1428−1434.
(62) Zeng, Y.; Wang, Y.; Liu, Y.; Dai, L.; Wu, Q.; Xia, M.; Zhang, S.; Ke, L.; Zou, R.; Ruan, R. Microwave Catalytic Co-Pyrolysis of Waste Cooking Oil and Low-Density Polyethylene to Produce Monocyclic Aromatic Hydrocarbons: Effect of Different Catalysts and Pyrolysis Parameters. *Sci. Total Environ.* **2022**, *809*, 152182.
(63) Naji, S. Z.; Tye, C. T.; Abd, A. A. State of the Art of Vegetable Oil Transformation into Biofuels Using Catalytic Cracking Technology: Recent Trends and Future Perspectives. *Process Biochem.* **2021**, *109*, 148−168.
(64) Arita, S.; Nazarudin, N.; Rosmawati, R.; Komariah, L. N.; Alfernando, O. The Effect of Combined H-USY and ZSM-5 Catalyst in Catalytic Cracking of Waste Cooking Oil to Produce Biofuel. *AIP Conf. Proc.*; AIP Publishing LLC: 2020, *2242* (June). doi: DOI: 10.1063/5.0007867.
(65) Elemental-Composition-of-MMT-Na-MMT-Ca-MMT-and-Cu-MMT-Obtained-from-XPS-Analysis.
(66) Fréty, R.; Rocha, M. D.; Brandão, S. T.; Pontes, L. A.; Padilha, J. F.; Borges, L. E.; Gonzalez, W. A. Cracking and Hydrocracking of Triglycerides for Renewable Liquid Fuels: Alternative Processes to Transesterification. *J. Braz. Chem. Soc.* **2011**, *22*, 1206−1220.
(67) Daroughegi, R.; Meshkani, F.; Rezaei, M. Enhanced activity of CO_2 methanation over mesoporous nanocrystalline Ni−Al_2O_3 catalysts prepared by ultrasound-assisted co-precipitation method. *Int. J. Hydrogen Energy* **2017**, *42*, 15115−15125.
(68) Lin, J.; Ma, C.; Luo, J.; Kong, X.; Xu, Y.; Ma, G.; Wang, J.; Zhang, C.; Li, Z.; Ding, M. Preparation of Ni based mesoporous Al_2O_3 catalyst with enhanced CO_2 methanation performance. *RSC Adv.* **2019**, *9*, 8684−8694.
(69) Urbanek, O.; Sajkiewicz, P.; Pierini, F. The effect of polarity in the electrospinning process on PCL/chitosan nanofibres structure, properties and efficiency of surface modification. *Polymer* **2017**, *124*, 168−175.

https://doi.org/10.1021/acsomega.1c06518
ACS Omega 2022, 7, 4585−4594